HEWLETT PACKARD

High Power Semiconductor Edge-Emitting Light Emitting Diodes for Optical Low Coherence Reflectometry

Julie Fouquet, Gary Trott, Wayne Sorin
Instruments and Photonics Laboratory
Mike Ludowise, Solid State Technology Laboratory
David Braun, Microwave Technology Division
HPL-94-54
June, 1994

OLCR, low coherence reflectometry, precision reflectometry, edge-emitting LED, EELED, incoherent, OCDR

A new semiconductor source was designed for optical low coherence reflectometry, increasing the sidelobe-free dynamic range by three to five orders of magnitude compared to conventional EELEDs. Reflectivities internal to an optical fiber circuit separated by as much as eight orders of magnitude can now be detected at wavelengths of 1.3 and 1.55 μm using compact semiconductor sources. In addition, nearly 1 mW of optical power with a smooth spectrum at a wavelength of 1.5 μm was coupled into single mode fiber at a 200 mA drive current near 0°C.

Internal Accession Date Only

Introduction

Optical reflectometry techniques of various types have been used for years to characterize optical fibers and circuits [1]. Optical time-domain reflectometry (OTDR) can locate breaks tens of kilometers away from the reflectometer by measuring the time elapsed between sending a short pulse and receiving its reflection. Sophisticated pulse coding sequences have improved performance, reducing measurement time by over an order of magnitude [2]. However, to make high spatial resolution (~50 μm) measurements over short distances (~1 m), OTDR would be impractical due to fiber dispersion limitations and detector bandwidth limitations. In this regime, optical low coherence reflectometry (OLCR), also known as optical coherence domain reflectometry [3], is generally more practical. This technique has been used for optical fiber circuit applications as well as for biological applications such as imaging within an eye [4] and probing through tissue [5].

OLCR is based on interference using a low coherence source in a Michelson interferometer. The source is coupled into an optical fiber and split in a 3 dB coupler, as illustrated in Fig. 1. Half of the signal goes to a device under test (DUT), while the other half is launched into free space towards a mirror on a scanning translation stage. When the optical path length to the mirror equals the optical path length to a reflection in the DUT, the signals from the two arms add coherently to produce a coherence spike at the detector located on the fourth arm of the coupler. When the optical path length difference becomes larger than the coherence length of the source, the interference signal no longer exists. The amplitude of the coherence signal is proportional to the reflection coefficient of the feature in the DUT. Translating the mirror allows the reflectivity profile of the DUT to be mapped.

The resolution of this technique is high enough to distinguish a pair of reflections within the DUT physically separated by 20 μm (in air) at 1.3 μm wavelength. At 1.55 μm, the

difference in dispersion between air in the translating mirror arm and optical fiber in the DUT arm limits resolution to roughly 50 μm over 40 cm lengths with edge-emtting light emitting diode (EELED) sources [6].

OLCR can measure extremely weak reflections, below -145 dB, with a high power source such as amplified spontaneous emission in a laser diode-pumped Er-doped single mode fiber at 1.55 μm [7]. Such a source is expensive, however, and current technology does not allow a practical extension of this high performance to the low dispersion wavelength of 1.3 μm. For these reasons, direct low coherence semiconductor sources are needed. Ideally, such sources would couple high powers into single mode fibers for high signal-to-noise ratios, but with a very low degree of coherence. (Single mode fiber is typically used in order to avoid degradation of resolution due to modal dispersion.) This set of properties is atypical. Lasers can output large powers (>1 mW/nm) into single mode fiber, but with high coherence. Superluminescent light emitting diodes (SLDs) can output powers on the order of 100 μW/nm, but typically have unacceptably large sidelobes due to relatively strong internal reflections. Tungsten-filament light bulbs have low coherence, but only very low powers (~1 nW/nm) can be coupled from them into single mode fibers [8].

Semiconductor EELEDs are currently capable of coupling more low-coherence power into a single mode fiber at 1.3 and 1.55 μm than surface-emitting LEDs [9]. OLCR sources must have very low internal reflections, however. Despite relatively smooth spectra, commercially-available non-superluminescent EELEDs contain internal secondary reflection sidelobes which range from -30 to -55 dB, much larger than ideal.

Reflections within an EELED may be characterized by using the EELED as the OLCR source and using a second mirror as the DUT. The position of the first mirror is translated while the second mirror remains stationary in order to map the positions of the internal

reflections. A small fraction of the primary output reflects off the front facet of the device, then reflects a second time off some other feature within the device, e.g. the back facet, so that this secondary signal travels in the same direction as the primary output but is delayed in time. These secondary reflected signals are amplified in the gain region of the device. The resulting sidelobes appear when the optical path length difference between the two mirrors equals the optical round trip distance between the reflections inside the device. They are undesirable artifacts, masquerading as true reflections within the DUT and confusing the interpretation of the reflection profiles. Secondary reflection signals may also be generated if the primary output reflects off an external lens or other surface, then again off the front facet of the device. These external reflection signals can be controlled by standard techniques, however; our primary concern in this work is reflections internal to the EELED.

Powers coupled from commercial EELEDs into single mode fibers tend to be low, from 2 to 50 μW at 1.55 μm. Powers tend to be lower at 1.55 μm than at 1.3 μm, presumably due to higher Auger recombination losses [10]. Since photon shot noise often limits reflectometer sensitivity, higher EELED output powers can extend the dynamic range of a reflectometer. Thus an optimal EELED source for reflectometry would couple high output power into single mode fiber with no detectable sidelobes due to internal reflections.

Here we report new EELEDs at 1.3 and 1.55 μm with sidelobes below -80 dB. This design improves the usable dynamic range of 1.55 μm OLCR by approximately three to five orders of magnitude. The 1.55 μm devices can output over 40 μW into single mode fiber with -81 dB internal reflection sidelobes and over 220 μW into single mode fiber with -55 dB sidelobes. The design of these devices is discussed below.

These EELEDs can also be operated at low temperatures to produce powers as high as 1 mW coupled into single mode fiber. The sidelobes in this case are too large for high sensitivity OLCR. However, broad spectral width sources which can couple high powers into single mode fibers are useful for other measurements, including near-infrared absorption.

Device Design

A smooth, continuous, constant cross-section waveguide geometry is desirable because even a small change in cross section along a waveguide can induce a reflection by changing the effective refractive index. For example, a 0.01 change in refractive index in a typical InGaAsP waveguide yields a -57 dB reflection. Two separate contacts were deposited on top of the waveguide. The region under the front contact produced light under forward bias. The region under the back contact functioned as a long absorber to attenuate the reflection signal off the back facet of the device. A reverse bias could be applied to this back contact to reduce the bandgap of the absorber to an energy below the bandgap of the gain region [11] through either the quantum-confined Stark effect (QCSE) [12] (for quantum wells) or the Franz-Keldysh effect [13] (for a bulk active region), further increasing the absorption. Besides attenuating the backward traveling signal from the gain region, this absorber can make the EELED more stable by attenuating any light accidentally injected into the back facet of the device. This design is useful in other applications as well. Since QCSE absorption is considerably stronger than loss mechanisms in most conventional EELEDs it blocks lasing more effectively, even at low temperatures.

The device geometry is illustrated in Fig. 2. Under normal operation, the front contact is forward-biased to generate and amplify light, while the back contact is reverse-biased to prevent reflections from the back facet and exterior surfaces behind the device. A 100 μ

m-long unbiased section separates the gain and absorber regions. The epitaxial contact material lies away from the optical field, and thus can be removed to increase the impedance between the two top contacts to ~ 10 kΩ, which in turn reduces the leakage current between them to ~ 1 mA. The uncontacted region is long compared to that of a multi-section laser, so metal photolithography is not critical. The absorbing behavior of this region is consistent with the purpose of the present device.

Distributed reflections were observed to emanate from along the length of the active region in our early devices. As will be described below, we determined that the distributed reflections were due to sidewall roughness of the active region of the waveguide. An etch process was developed to yield very smooth sidewalls.

All the reflection sidelobes we observed involved an even number of reflections internal to the LED; the resulting signal had to travel in the same direction as the main signal in order to be measured using OLCR. The front facet was responsible for one of each pair of reflections. Therefore, a very low reflectivity front facet anti-reflection (AR) coating is critical to reduce the magnitude of all reflection sidelobes. We deposited a high precision, broadband AR coating on the front facet.

All output signal power must be developed during a single pass, since reflections for multiple passes yield sidelobes in the OLCR output. Single pass output power from a broad stripe EELED with an AR-coated front facet can be calculated by considering light emitted from a small volume of length Δx along the gain region, as shown in Fig. 3. The single pass output power in each polarization due to light originally generated in that short volume can be written as a sum over modes

$$\sum_i P_{noise-i} e^{\Gamma_i (g_i - \alpha_i) x} \qquad (1)$$

where $P_{noise-i}$ is the spontaneous emission power from that small volume which couples into the ith waveguide transverse mode, and the exponential term describes the single pass gain of the ith mode. Γ_i is the confinement factor, g_i is the gain per unit length, and α_i is the internal loss per unit length, all for the ith mode. x is the distance from the front facet of the device. $P_{noise-i} = P_{spon} wt \Delta x \eta_i(w,t)$, where P_{spon} is the spontaneous emission power density per unit volume, w is the lateral width, t is the height of the active region, and $\eta_i(w,t)$ represents the fraction of spontaneous emission coupled into the ith mode in the forward direction, which depends on geometry. Summing the contributions from all the transverse modes and letting $\Delta x \to 0$ to integrate along the gain region, we have

$$P_{out-mm} = \sum_i P_{spon} wt \eta_i(w,t) \int_0^{L_g} e^{\Gamma_i (g_i - \alpha_i) x} dx \qquad (2)$$

where P_{out-mm} is the single pass output power of the multi-transverse mode EELED and L_g is the length of the gain region. Here we have assumed that a high quality AR coating on the output facet transmits all internal light incident on the facet. After integrating and defining $G_i \equiv e^{\Gamma_i (g_i - \alpha_i) L_g}$ we obtain

$$P_{out-mm} = \sum_i \frac{L_g P_{spon} wt \eta_i(w,t)}{\ln(G_i)} [G_i - 1] \qquad (3)$$

This equation shows that large L_g, $\Gamma_i(g_i - \alpha_i)$ and P_{spon} all contribute to high P_{out}. Increasing w, t, $\eta_i(w,t)$ and the number of modes also helps to generate the highest multimode power. Our devices used a thickness, t, typical for single transverse mode lasers. The lateral design was a semi-insulating planar buried heterostructure (SIPBH) [14], whose high refractive index difference between the active region and surrounding InP yields good values for the $\eta_i(w,t)$. The mask stripewidth, w, was varied in practice from narrow to wide values compared to the maximum value allowed for single mode operation.

Because our optical low coherence reflectometer uses single mode fiber, it is more important to generate a large amount of power in the fundamental mode, which will be coupled into the fiber, than to maximize the power in all modes. The single mode output power, $P_{out\text{-}sm}$, has the same dependence on G as above

$$P_{out-sm} \propto \frac{P_{spon} L_g}{\ln(G)}[G-1] \tag{4}$$

where the subscripts for the lowest order mode have been dropped. The SIPBH design has good optical confinement Γ, good current confinement for high g and no absorption loss in metal or unpumped areas for low α. Auger (nonradiative) recombination worsens with increasing temperature, so this structure is also beneficial because it effectively conducts heat away from the active region to yield a higher G and P_{spon}. To increase further the single pass gain, a relatively long gain region of approximately 800 μm was used. The relatively wide well thicknesses in the QW devices tend to control Auger recombination (which increases as the third power of the carrier density) because carrier densities are lower for larger well volumes. A bulk rather than quantum well active region was employed to obtain the highest output powers, however; the larger active region volume of bulk material as compared to QW material yielded a lower carrier density for equivalent currents.

Device Fabrication and Testing

Our EELED, shown in Fig. 2, uses a two-growth SIPBH process adapted from a similar laser process which has produced 300 μm-long 1.3 μm lasers with 15 mA dc room temperature thresholds in our laboratory. The quantum well (QW) and bulk active region devices both used a similar double heterostructure epilayer design grown by metalorganic chemical vapor deposition (MOCVD). All layers were nominally lattice matched to InP. The substrates were InP:S. The epitaxial layers were 1.5 to 1.75 μm-thick *n*-doped InP

lower cladding, active, 2.3 to 2.4 μm-thick *p*-doped InP:Zn upper cladding, and 0.15 to 0.19 μm-thick *p*-doped contact. The 1.5 μm-emitting devices also included a final 0.12 μm-thick InP layer to improve SiO_2 adhesion, which was removed later during processing.

The active regions of all the EELEDs were not intentionally doped. For the 1.3 μm-emitting EELEDs, the active region comprised a 200 nm separate confinement heterostructure (SCH) layer, four quaternary QWs (L_z = 9 nm) and three barriers (L_b ~ 20 nm), and a 200 nm SCH layer. The SCH and barrier layers are composed of $Ga_{1-x}In_xAs_{1-y}P_y$ with a bulk bandgap corresponding to an emission wavelength (λ_g) of 1.1 μm. The QW $Ga_{1-x}In_xAs_{1-y}P_y$ material's λ_g was1.4 μm. For the 1.5 μm-emitting bulk EELEDs, the active region was a 0.2 μm-thick $Ga_{1-x}In_xAs_{1-y}P_y$ layer with composition emitting at 1.55 μm. For the 1.5 μm-emitting QW device, the active region consisted of a 120 nm $Ga_{1-x}In_xAs_{1-y}P_y$ λ_g=1.2 μm SCH layer, four ternary GaInAs QWs (L_z ~ 7.5 nm) separated by three barriers (L_b ~ 10 nm), and a 120 nm SCH layer, both with λ_g=1.2 μm.

An SiO_2 layer was deposited next. Photolithographic mesa stripes were patterned on the SiO_2, and the SiO_2 was etched. The photoresist was removed, and the SiO_2 was used as an etch mask to create the mesa stripes.

The mesa stripes in the 1.3 μm EELEDs were defined by a selective wet etch sequence similar to that described by Chakrabarti and Agrawal [15]. However, the combination of wet etches through the SiO_2 and epitaxial layers tends to undercut the SiO_2 etch mask unevenly, leading to mesa sidewall roughness. A new etch process was developed to yield smoother mesa sidewalls for the 1.5 μm devices. The InP cap and the contact layers were removed using a 12 sccm CH_4 / 60 sccm H_2 / 30 sccm Ar reactive ion etch at 15 mTorr. Next the wafer was etched in O_2 for 30 minutes at 40 sccm and 3 mTorr to remove any carbon-based polymers on the wafer. As long as the etch penetrates into the InP upper cladding layer, the precise etch depth is not critical. At this stage, a small (~0.1 μm)

sidewall roughness is visible using scanning electon microscopy. Next a selective wet etch (the InP etch in [15]) was used to remove the InP upper cladding layer, stopping at the active region. The contact layers serve as the mask for this etch, which tends to smooth out sidewall roughness after the reactive ion etch step. The sidewalls were completely smooth after the wet InP etch, as shown in Fig. 4. Because the sidewall profile is reenterant, the active region is narrower than the original mask stripewidth. Unfortunately, the wet etch also aggressively removed the InP cap layer. A final 10 sec wet etch in a nonselective 4% Br / methanol solution at room temperature was used to remove the active region from the field, as well as residual damage caused by the reactive ion etching. This etch aggressively attacked the exposed top corners of the InGaAs contact layer, significantly reducing its width and resulting in a small amount of sidewall roughness.

Semi-insulating InP:Fe was regrown at a temperature of approximately 575°C around the mesa with ferrocene flow stepped up from 0 to 10 sccm. The InP:Fe confines the current to the active region while providing optical confinement and good thermal conduction from the active region. After removal of the SiO_2 stripes, photoresist was patterned for separate gain and absorber contacts. *p*-metal contacts consisting of 100 nm Ti / 150 nm Pt / 200 to 300 nm Au were evaporated on the top of the wafer and metal was lifted from the field when the photoresist was removed. The wafer was backlapped and polished to a final thickness of about 100 μm, and a continuous Ni / 12%Ge-88%Au or Ni / Pt / Au *n*-metal contact was evaporated over the entire backside of the wafer and alloyed for 15 sec at 380°C on a strip heater. The GaInAs etch described in [15] for approximately 10 seconds was used to separate the epitaxial contact material between the front and back contacts of the 1.5 μm EELEDs; this step was carried out before the backlap for the 1.3 μ m EELEDs.

Both the front and back facets of the EELED are cleaved similarly to a laser. The processed wafers could be cleaved in two ways. The shorter (1.3 mm-long) devices contain a continuous waveguide with a 300 μm-long forward-biased gain contact and an 880 μm-long reverse-biased absorber contact separated by a100 μm-long unbiased gap. An unbiased region approximately 20 μm long is present at the absorber end, just before the back facet. The longer (2.6 mm) devices contained an 800 μm-long gain contact followed by multiple absorber contacts, the first one 880 μm long. A 1.5 μm-emitting QW laser 600 μm long cleaved from the edge of the same wafer had a rather high threshold current of 38 mA.

A three-layer antireflection (AR) coating was deposited on the output facet of the cleaved EELEDs. Our design was based on a two-layer approach, which yields a single broadband minimum in contrast to the narrowband minimum of a single layer AR coating. Actually, two layers were used to simulate what would normally be a single bottom layer in order to obtain the required refractive index, making a total of three layers. Coating designs were optimized separately for 1.3 and 1.5 μm wavelengths. The application of the AR coating reduced output facet reflection sidelobe magnitudes by 25 to 30 dB.

For testing of internal reflections, a DC current source drives the forward-biased gain contact, while a negative voltage is applied to the absorber contact. The EELED is coupled into a single mode fiber via a single, non-optimized gradient index lens to serve as the source in the OLCR measurement. The amount of output power from the device which can be coupled into single mode fiber depends on the device and drive current, but is very roughly an order of magnitude smaller than the output power into air. This coupling efficiency is low compared to lasers. Improvements in coupling should be possible. Unless otherwise noted, powers reported are powers after coupling into single mode fiber. The light is split in a 3 dB fiber directional coupler and enters the two arms: a mirror on a translation stage terminates the reference arm, and a bare fiber end or mirror

replaces the DUT in the other arm. Reflected signals are recombined in the coupler and travel to a detector. Ideally only a single interference signal should appear from each feature in the DUT as the mirror is translated. However, multiple round trip reflections inside the EELED source can cause interference sidelobes when the optical path length difference between the two mirrors matches the optical round trip distance between the internal reflections. In OLCR these undesirable source reflections appear as low level sidelobes placed symmetrically around the main single pass output of the EELED.

Results and Discussion

The OLCR output with a mirror as the DUT of an early 1.3 μm QW EELED prior to antireflection coating the front facet is shown in Fig. 5. The gain contact is forward-biased at 75 mA dc and the absorber contact is open. The central peak in this figure is the desired single pass output of the EELED and for an ideal device only this single, narrow peak would be visible. The other peaks are undesirable sidelobes due to internal reflections. The distributed signal (a) at -52 to -66 dB below the main peak is the result of reflections between the front facet and scattering in the gain region of the EELED. Reflection signals from the far end of the gain region are larger in amplitude, presumably because they travel farther along the gain region and thus experience more amplification. They are probably due to mesa sidewall roughness because, first, the period of the indentations was large enough compared to the wavelength in the semiconductor to generate a reflection. In contrast, grown epitaxial interface roughness was far too small compared to the emission wavelength to contribute significant reflections. Second, the amplitude of this distributed reflection signal decreased by 18 dB as mesa stripewidth was increased from five to eight μm, even as the amplitude of the main peak increased over most of this range. Since the fundamental mode's wavefunction interacts less with the mesa edge for a wider mesa, a lower reflection signal would be expected. The peak at the end of this region, (b), about 52 dB down, comes from the region between the gain

and absorber contacts and may result from the refractive index discontinuity due to the difference in carrier density between the forward-biased gain region and the reverse-biased absorber, or from a possible waveguide discontinuity caused by accidental etching into the InP upper confinement layer during processing.

The separate peak (c) at -49.5 dB in Fig. 5 comes from the back facet of the device. To first order, the emission spectrum of the forward-biased gain region peaks at the same wavelength as the absorption edge in the unbiased absorber. Emission from the gain region at wavelengths longer than the absorption edge can pass through the unbiased absorber, reflect off the semiconductor-air interface at the back facet and pass back through the absorber in the reverse direction with relatively little attenuation.

When a sufficient reverse bias voltage is applied to the absorber, the QCSE moves the absorption edge to a longer wavelength, which blocks the long wavelength gain emission. Figure 6 illustrates how the amplitude of the sidelobe due to reflection at the back facet is reduced with increasing reverse bias voltage magnitude for a device with a 300 μm-long gain region and a 880 μm-long absorber contact. The sidelobe decreases by over 35 dB when a 4 V reverse bias is applied, falling to 85 dB below the main peak [11]. This level is far lower than sidelobe levels we have measured on commercially available GaInAsP EELEDs.

Emission from the absorber end of a 1.3 μm device is shown in Fig. 7. Here a fixed 50 mA forward current drives the gain region, while the back contact is driven over a wide range of conditions, from a forward current of 75 mA in curve (a) to 1 mA in curve (d). The absorber is left open for curve (e) and biased from 0 (short circuit) to -3 V for curves (f) through (h). Emission from the gain region is greatly attenuated by the reverse bias. The peak wavelength increases over 100 nm through the full range of bias conditions, graphically illustrating the quantum confined Stark effect. An abrupt loss of short

wavelength emission is observed when the nominal absorber is no longer forward biased, from curves (d) to (e) [11]. If a bulk active region is used, the Franz-Keldysh effect attenuates the back facet reflection signal when the absorber is reverse-biased.

To reduce further the magnitude of the reflection signals in Fig. 5 (all of which include an internal reflection off the front facet), a multi-layer antireflection coating was deposited on the front facet of the EELED. Sidelobe magnitudes fell by an additional 25 to 30 dB. For a nominal -25 dB antireflection front facet coating, the sidelobe due to reflection off the back facet would be 110 dB below the main peak, lying below the noise floor in Fig. 5. The amplitude of this peak could be further reduced to less than 135 dB below the main peak by depositing a second antireflection coating on the back facet, but this action is unnecessary. The OLCR output of the antireflection-coated EELED is shown in Fig. 8 for 75 mA drive current [11]. This δ function-like reflectivity behavior is ideal for OLCR, but the 6 μW power coupled into single mode fiber (no heatsink) is lower than desired for the best signal-to-noise ratio.

Increasing the gain region length from 300 to 800 μm significantly increased the output power for the same current to the gain region, as shown for two otherwise similar, heatsunk 1.3 μm EELEDs in Fig. 9. The concave-upward current dependence for the long gain region device indicates that gain is present. Single mode fiber-coupled output power versus mask stripewidth w is shown in Fig. 10 for L_g=800 μm, 1.5 μm-emitting devices with smooth sidewalls and (a) bulk and (b) QW active regions before heatsinking. In both cases the optimal stripewidth was approximately 4 μm. This width is narrower than the 7 μm optimal stripewidth for earlier 1.3 μm-emitting L_g=300 μm devices with rougher sidewalls, presumably because the smoother sidewalls cause less scattering loss. As shown in Fig. 11, at low currents quantum wells (QWs) have higher gain than bulk material, enough that the QW EELED has slightly higher output power than its bulk counterpart despite the lower confinement factor. At higher currents, the bulk device has

the highest power both because of its higher confinement factor and since its lower carrier density causes less nonradiative Auger recombination. Lengthening the gain region and using appropriate higher drive currents should further increase the output powers of both types of devices.

The longer gain region devices suffered from larger reflection sidelobes, however; the higher gain amplified the undesired spurious reflection peaks as well as the desired single pass main peak. The absorber still blocked the back facet reflection signal well, but the distributed reflection signal was large. Since the signal reflected from the back end of the gain region experiences an extra round trip through the active region, its amplitude increases more rapidly with gain - and thus with drive current - than the single pass main signal does. Figure 12 shows the OLCR response of a 1.5 μm-emitting QW EELED with L_g=800 μm driven at 200 mA (heatsunk). The highest sidelobe was 81 dB down from the main single pass peak, the FWHM of the spectrum was 89 nm, and the output power was 44 μW into single mode fiber. Both of the OLCR curves in Fig. 13 come from the same bulk 1.5 μm-emitting device driven at two different gain region current levels (heatsunk). At 100 mA current, approximately 22 μW was coupled into single mode fiber and the OLCR output showed only small spurs 78 dB down. At 200 mA drive current, the output power increased to 224 μW with good coupling to single mode fiber, but the maximum distributed reflection signal increased to 55 dB below the main single pass peak. The spectrum was smooth, with a 44 nm FWHM. The dependence of reflection performance on drive current obfuscated comparisons between both different devices and descriptions of individual devices. In order to evaluate the reflection performance of EELEDs independent of current, a figure of merit was developed.

The largest distributed reflection signal, P_{dist}, generally comes from the back end of the gain region:

$$P_{dist} = P_{out} R_{oc} G R_{dist} G \propto G^2 \tag{5}$$

where R_{oc} is the output facet reflectivity and R_{dist} is the effective reflectivity of the distributed reflection. This G^2 dependence needs to be balanced with an easily measureable value in order to reduce the current dependence. Since P_{out} is roughly proportional to G, it was used to yield the following figure of merit:

$$F \equiv 2P_{dB} + E_{dBc} \tag{6}$$

where P_{dB} can conveniently be referenced to 1 mW as

$$P_{dBm} = 10 \times \log_{10}\left(\frac{P_{out}}{1mW}\right) \tag{7}$$

The extinction coefficient E_{dBc} is given by

$$E_{dBc} = 10 \times \log_{10}\left(\frac{P_{out}}{P_{dist}}\right) \tag{8}$$

which is a positive number. The figure of merit can be divided into constant and weakly current-dependent terms

$$F = 10\left[K + \log_{10}\left(\frac{1}{R_{oc}R_{dist}}\right) + \log_{10}\left(\frac{(G-1)^2}{G^2}\frac{L_g^2}{(\ln G)^2}\right)\right] \tag{9}$$

where the constant K depends on the reference power. The measured figure of merit F is plotted as a function of current in Fig. 14 for various high power devices. The 1.5 μm-emitting EELEDs have 4 μm mask stripewidths. The 1.3 μm-emitting devices had rougher sidewalls, producing higher output power for wider stripewidths; thus an 8 μm stripewidth was used. (Recall that wider stripe devices show weaker distributed reflection sidelobes than narrower stripes from the same bar.) The current dependence in Fig. 14 is weak enough to allow clear evaluation of the spur performance of the different EELEDs.

The figures of merit at high currents largely represent the quality of the AR-coatings. Companion bulk lasers in the AR-coating runs indicated that the run for the 1.5 μm-emitting QW EELED had the lowest reflectivity, while the 1.5 μm-emitting bulk EELED had the highest and the 1.3 μm-emitting EELED fell in between.

Cooling below room temperature increased output power in both devices, as shown in Fig. 15. At a temperature of 0°C, 0.95 mW was coupled from the bulk EELED into single mode fiber. The bulk design benefited significantly more from cooling than the QW design. This behavior is consistent with the explanation that the higher carrier density in the QW device causes more Auger recombination.

Output spectra were smooth as seen on an optical spectrum analyzer, even for the highest powers, but at these very high powers the distributed reflection sidelobes grew to an amplitude 37dB below the main peak. Also, instead of terminating at the end of the gain region, these reflection signals were measured to extend roughly 400 μm into the absorbing region. This result indicates that the absorber is saturating near the gain region. The spectral FWHM was approximately 40 nm, as shown in Fig. 16.

While the -37 dB distributed reflection signal rules out the use of this cooled device in high dynamic range OLCR, other applications are possible. Typical high power edge-emitting LEDs are superluminescent, utilizing reflections to generate sub-threshold stimulated emission. Such devices generally have strongly modulated spectra. These peaks make the devices unsuitable for many measurements, e.g. absorption spectroscopy. The smooth spectrum device with a 1 mW output presented here enables absorption spectroscopy as well as many other types of measurements. This device should also be relatively immune to external reflections, unlike amplifiers and near-threshold superluminescent LEDs.

Conclusion

In summary, internal reflection sidelobes were reduced to extremely low levels in semiconductor edge-emitting light emitting diodes at 1.3 and 1.55 μm. Back facet reflection signals were suppressed using an integral reverse-biased absorber through either the quantum-confined Stark effect or the bulk Franz-Keldysh effect. The source of distributed reflection signals from the gain region was identified as roughness of the active region sidewalls, allowing reduction of these reflection signals through process control. Deposition of an AR coating on the front facet further reduced all sidelobes due to internal reflections. Single-pass gain resulted in high output powers in devices having 800 μm-long gain regions. Sidelobes in QW EELEDs were reduced to less than -80 dB at 1.56 μ m, with powers over 40 μW coupled into single mode fiber. Coupled powers over 220 μ W were obtained in room temperature bulk active region EELEDs with approximately -55 dB sidelobes. At temperatures near 0°C, coupled power increased to near 1 mW with a 40 nm-wide smooth spectrum. These EELEDs increase the usable dynamic range in optical low coherence reflectometry measurements by three to five orders of magnitude.

The authors acknowledge assistance from H. Gamino, S. Close, J. Ratcliffe, B. Perez, B. Borsberry, B. Kendle and N. Andring. Useful discussions with and die-attach assistance from D.J. Derickson are acknowledged. Support from K.W. Carey and R. Moon is appreciated.

References

1. P. Healey, "Review of Long Wavelength Single-Mode Optical Fiber Reflectometry Techniques," *J. Lightwave Technology*, vol. LT-3, pp. 876-886, 1985.

2. M. Nazarathy, S.A. Newton, R.P. Giffard, D.S. Moberly, F. Sischka, W.R. Trutna, Jr. and S. Foster, "Real-Time Long Range Complementary Correlation Optical Time Domain Reflectometer," *IEEE J. Lightwave Technology*, vol. 7, pp. 24-38, 1989.

3. R.C. Youngquist, S. Carr and D.E.N. Davies, "Optical Coherence-Domain Reflectometery: A New Optical Evaluation Technique," *Opt. Lett.*, vol. 12, pp. 158-160, 1987.

4. D. Huang, E.A. Swanson, C.P. Lin, J.S. Schuman, W.G. Stinson, W. Chang, M.R. Hee, T. Flotte, K. Gregory, C.A. Puliafito, and J.G. Fujimoto, "Optical Coherence Tomography," *Science*, vol. 254, pp. 1178-1181, 1991.

5. X. Clivaz, F. Marquis-Weible, R.P. Salathe, R.P. Novak and H.H. Gilgen, "High-Resolution Reflectometry in Biological Tissues," *Optics Letters*, vol. 17, pp. 4-6, 1992.

6. H. Chou and W.V. Sorin, "High-Resolution and High-Sensitivity Optical Reflection Measurements Using White-Light Interferometry," *Hewlett-Packard Journal*, pp. 52-59, 1993.

7. W.V. Sorin and D.M. Baney, "Measurement of Rayleigh Backscattering at 1.55 μm with 32 μm Spatial Resolution," *IEEE Photonics Technology Letters*, vol. 4, pp. 374-376, 1992.

8. L.F. Stokes, "Coupling Light from Incoherent Sources to Optical Waveguides," *IEEE Circuits and Devices Magazine*, vol. 10, pp. 46-47, 1994.

9. K.-L. Chen and D. Kerps, "Coupling Efficiency of Surface-Emitting LED's to Single Mode Fibers," *IEEE J. Lightwave Technology*, vol. 5, pp. 1600-1604, 1987.

10. G.P. Agrawal and N.K. Dutta, Long-Wavelength Semiconductor Lasers, New York, Van Nostrand Reinhold, 1986.

11. J.E. Fouquet, W.V. Sorin, G.R. Trott, M.J. Ludowise, and D.M. Braun, "Extremely Low Back Facet Feedback by Quantum-Confined Stark Effect Absorption in an Edge-Emitting Light-Emitting Diode," *IEEE Photonics Technology Letters*, vol. 5, pp. 509-511, 1993.

12. D.S. Chemla, T.C. Damen, D.A.B. Miller, A.C. Gossard and W. Wiegmann, "Electroabsorption by Stark Effect on Room-Temperature Excitons in GaAs/GaAlAs Nultiple Quantum Well Structures," *Appl. Phys. Lett.*, vol. 42, pp. 864-866, 1983.

13. L.V. Keldysh, *Soviet Physics - JETP*, vol. 7, pp. 788+, 1958, and W. Franz, *Z. Naturforsch*, vol. 13a, pp. 484+, 1958, as cited in J.I. Pankove, Optical Processes in Semiconductors, New York, Dover, 1971.

14. B.I. Miller, U. Koren, and R.J. Capik, "Planar Buried Heterostructure InP/GaInAs Lasers Grown Entirely by OMVPE," *Elec. Lett.*, vol, 22, pp. 947-949, 1986.

15. U.K. Chakrabarti and G.P. Agrawal, "A Novel Three-Step Mesa Etching Process for Semiconductor Lasers and the Use of Monte Carlo Simulations for Active Width Control," *J. Appl. Phys.*, vol. 65, pp. 4120-4123, 1989.

Captions

Figure 1: An optical low coherence reflectometer consists of a low-coherence EELED coupled into optical fiber, a 3 dB directional coupler, a mirror on a translation stage, and a photodetector. A signal is recorded when the optical path length to the mirror equals the optical path length to the device under test (DUT). The amplitude of this signal is proportional to the reflection coefficient of the feature in the DUT.

Figure 2: The EELED contains a continuous waveguide with separate top contacts. The forward-biased gain region produces spontaneous emission and amplifies it during the single pass to the output. The absorber attenuates any signal traveling in the opposite direction, preventing round trip reflections.

Figure 3: Spontaneous emission at the back end of the gain region of a properly-operating EELED experiences more gain before it reaches the output of the device than spontaneous emission generated near the output.

Figure 4: This scanning electron microscope photograph shows very smooth sidewalls after the hybrid dry / wet etch of a 1.5 μm EELED, prior to the active region etch step.

Figure 5: An OLCR scan was taken using one of the 1.3 μm QW EELEDs described here as the source before depositing an AR coating on the front facet, and with no reverse bias applied to the absorber contact. The DUT was replaced by a single reflector. The features on either side of the main EELED signal peak come from reflections between the front facet and: (a) scattering in the gain region of the EELED, which is probably due to mesa sidewall roughness; (b) the region between the gain and absorber contacts; and (c) the back facet of the EELED.

Figure 6: Increasing the magnitude of the reverse bias voltage applied to the absorber causes the quantum-confined Stark effect to block increasingly longer wavelengths in this

1.3 μm EELED before AR coating. The magnitude of the sidelobe due to the back facet reflection signal, shown as peak (c) in Fig. 5, decreases as a result. This reflection falls to -85 dB at a bias of -4 V.

Figure 7: Emission spectra from the 50 mA forward-biased gain region through the absorber and out the back facet depend on the bias applied at the the back (normally absorber) contact: forward biases of (a) 75, (b) 10, (c) 5, (d) 1 and (e) 0 mA; reverse biases of (f) 0, (g) 1.5 and (h) 3 V. Applying a reverse bias decreases transmission and shifts the transmission peak to longer wavelengths by approximately 100 nm over the full range of conditions studied.

Figure 8: Adding a multi-layer antireflection coating to the front facet of a 1.3 μm EELED reduced all sidelobes by an additional 25 to 30 dB. No reflection signals are observed down to the noise floor, which is located over 80 dB below the main single pass peak. The back facet signal is estimated to be -110 dB or lower for -4 V absorber bias.

Figure 9: Power coupled into single mode fiber is considerably higher for a 1.3 μm QW EELED of 800 μm gain region length than for a similar device of 300 μm length at the same current. Since the abscissa is current rather than current density, the difference in performance is especially significant.

Figure 10: Power coupled into single mode fiber versus drive current to the 800 μm-long gain region for 1.5 μm EELEDs of different mask stripewidths, given in μm, before heatsinking. Overall, achievable powers were considerably higher for (a) bulk active region devices than for (b) QW active region devices. (Note different vertcal scales.)

Figure 11: Power coupled into single mode fiber versus drive current for 4 μm-wide, heatsunk bulk and QW EELEDs.

Figure 12: This OLCR scan was taken using the AR-coated, heatsunk, 4 μm-wide, 800 μ m-long, 1.5 μm-emitting QW EELED from Fig. 11 as a source and a reflector as DUT. The gain region was driven at 200 mA, and 44 μW power was coupled into single mode fiber. This higher output power has lowered the noise floor, so that very weak internal reflections are measured to be approximately 81 dB below the main single pass peak. This performance represents an improvement of 27 to 52 dB in semiconductor-based OLCR at 1.5 μm.

Figure 13: OLCR scans of a bulk device similar to the QW device described in Fig. 12. The distributed reflection from the gain region is much smaller for a gain region drive current of (a) 100 mA than for (b) 200 mA. The distributed reflection signal makes extra two-way trips through the gain region, which leads to high amplification at high currents.

Figure 14: The figure of merit described in the text is relatively independent of current as intended, allowing the reflection suppression properties of different devices to be compared. Some of the variations in performance can be attributed to the run-to-run variation of the AR coating reflectivity.

Figure 15: Power output into single mode fiber increases as the temperatures of the devices in Fig.s 11-13 are lowered, more so for the (a) bulk than the (b) QW EELED. (Note different vertical scales.) The difference may result from greater nonradiative Auger recombination due to higher carrier densities in the QWs.

Figure 16: At 5°C, the bulk device described in Fig. 14 couples a power approaching 1 mW into single mode fiber. The distributed reflections are also amplified to 37 dB below the main single pass peak, rendering the cooled device unsuitable for high sensitivity OLCR. Still, the spectrum of is smooth (FWHM > 40 nm), unlike spectra from superluminescent diodes typically used to achieve these output powers. This high power, broad spectrum source can be used in other applications such as absorption spectroscopy.

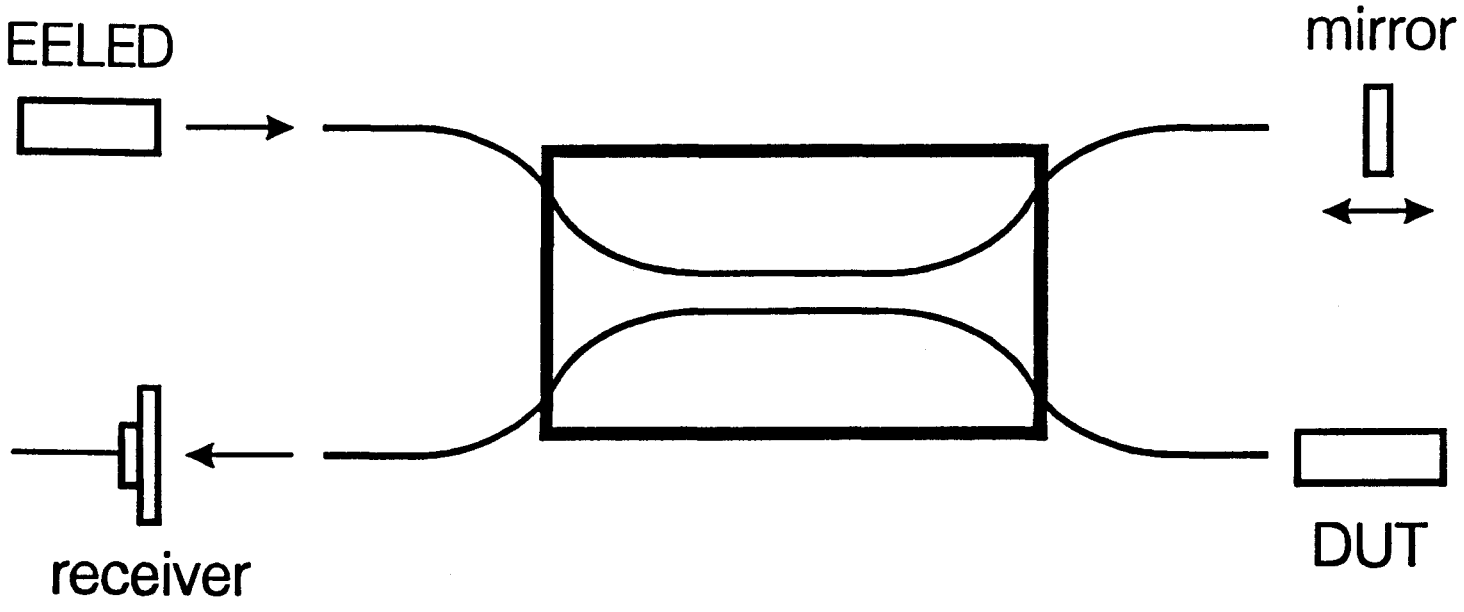

Figure 1

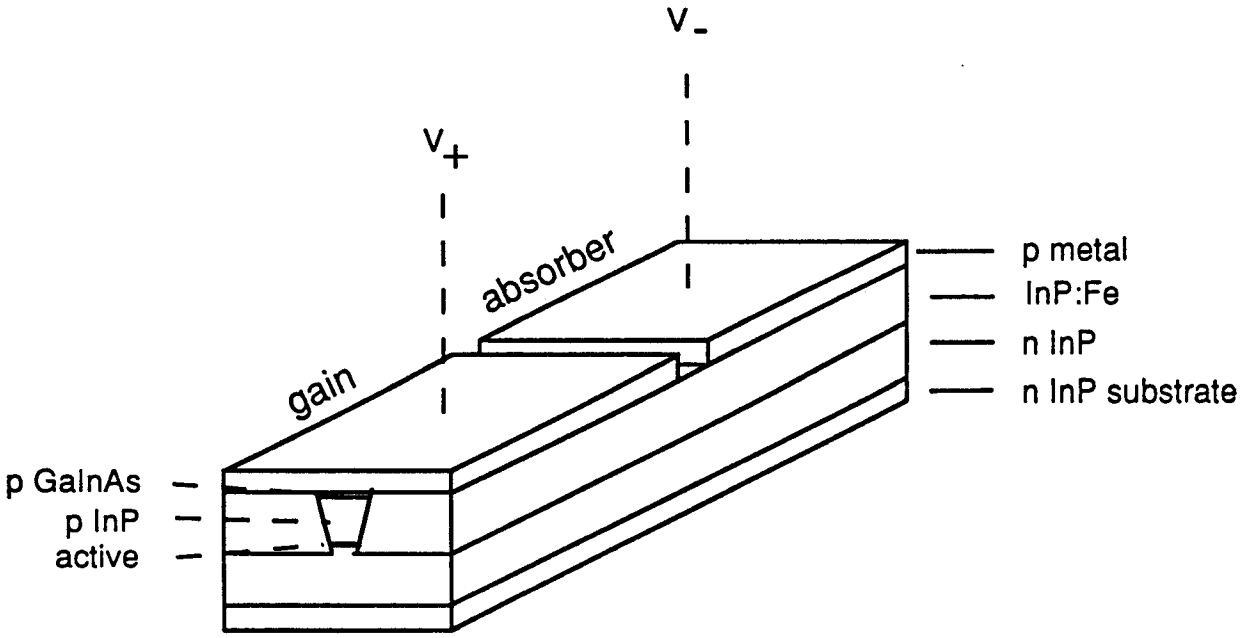
V-
V+
absorber
gain
p metal
InP:Fe
n InP
n InP substrate
p GaInAs
p InP
active

Figure 2

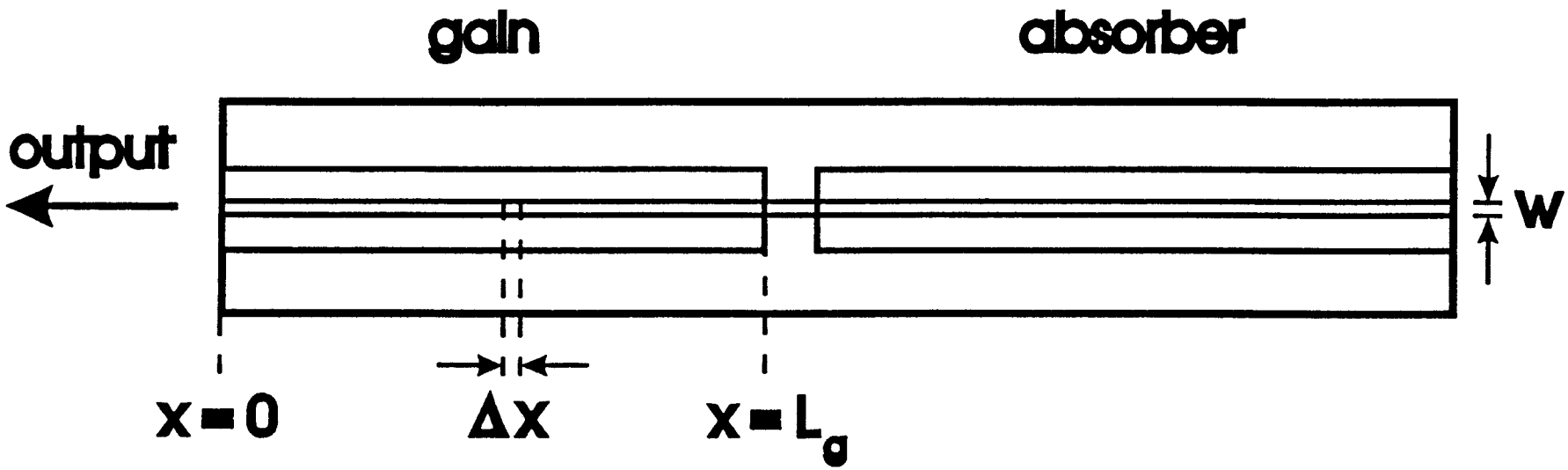

Figure 3

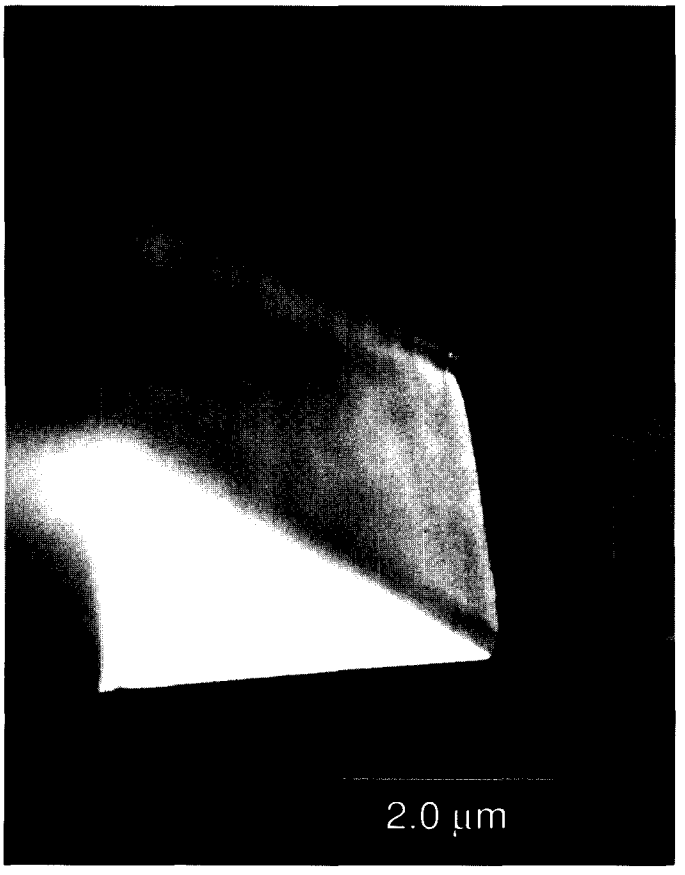

Mesa etched through p InP cladding.

Figure 4

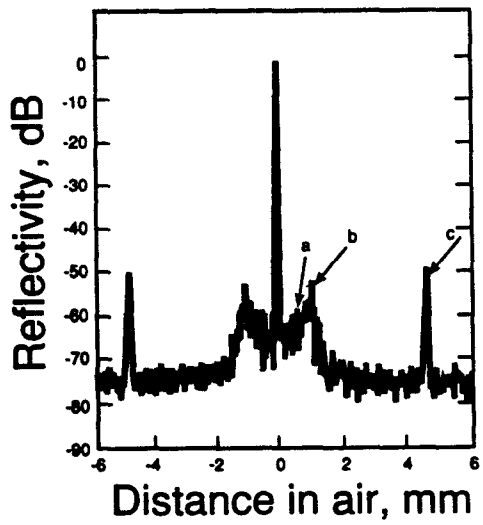

Figure 5

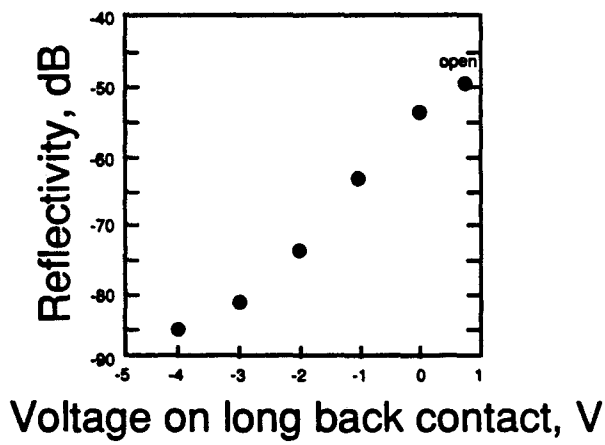

Figure 6

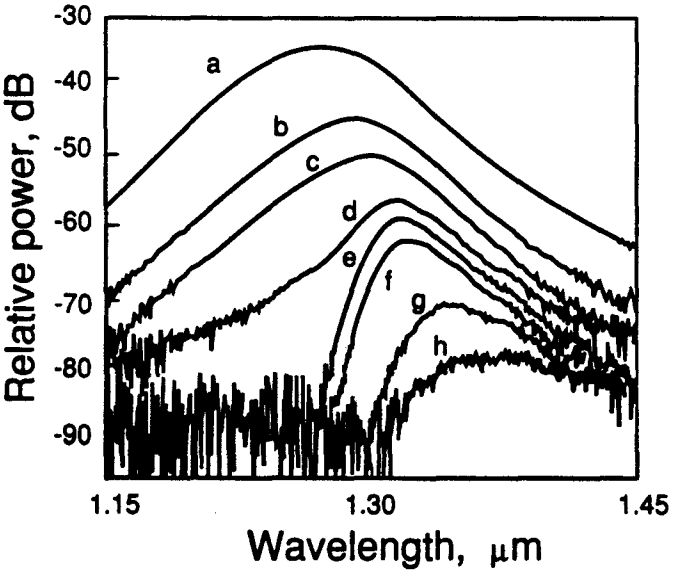

Figure 7

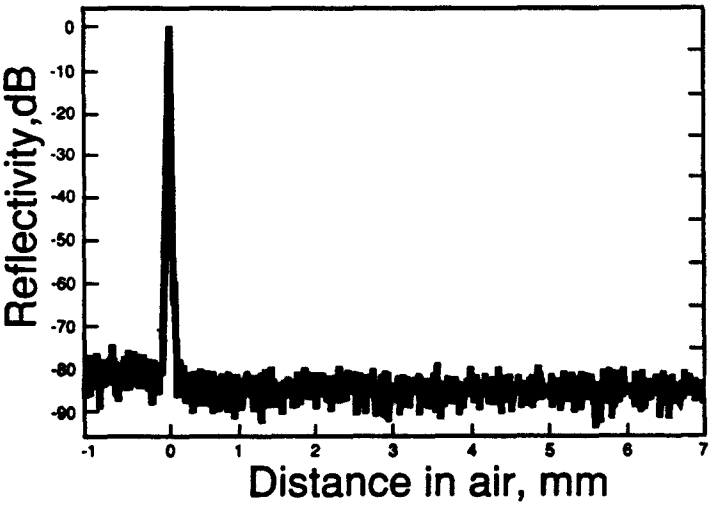

Figure 8

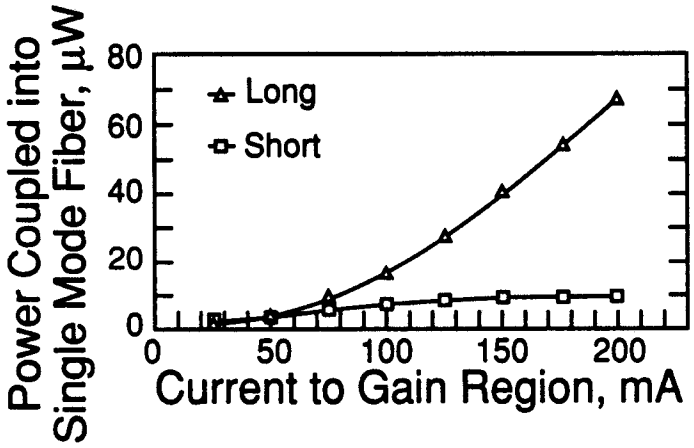
Power Coupled into
Single Mode Fiber, μW
80
60
40
20
0
Long
Short
0
50
100
150
200
Current to Gain Region, mA

Figure 9

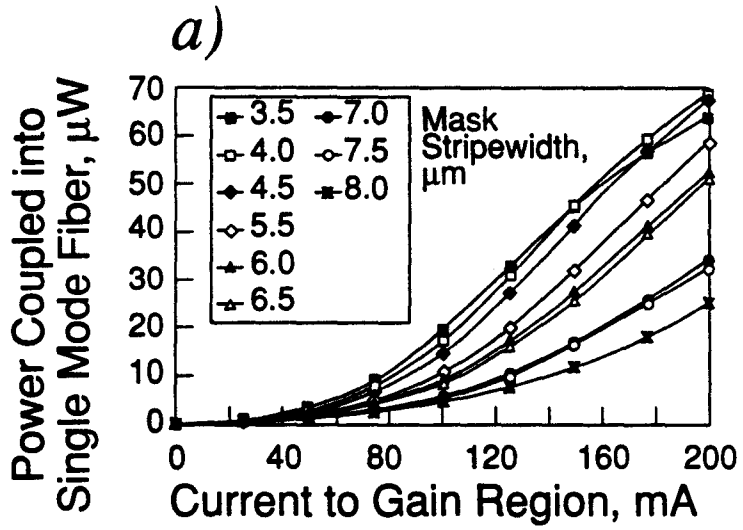

Figure 10a

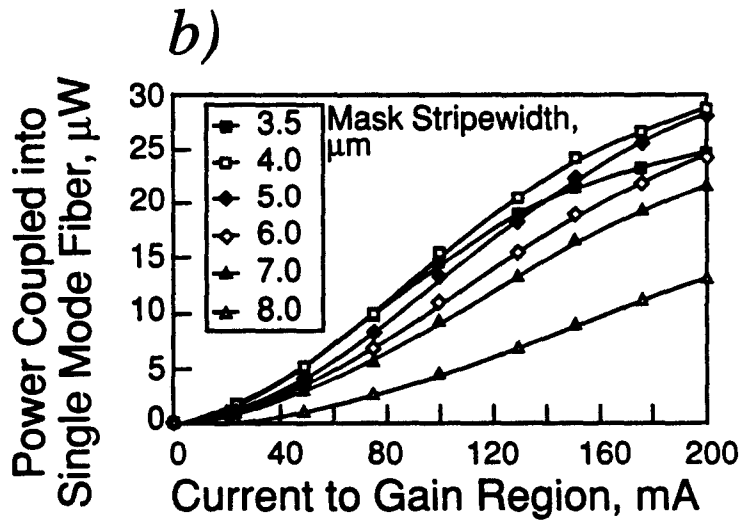

Figure 10b

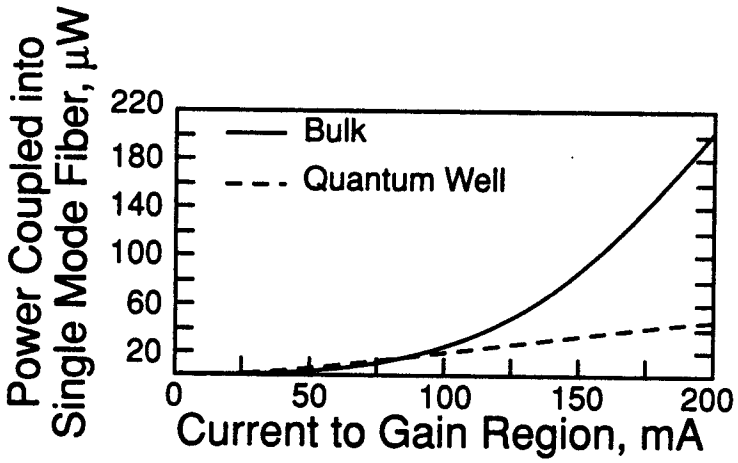

Figure 11

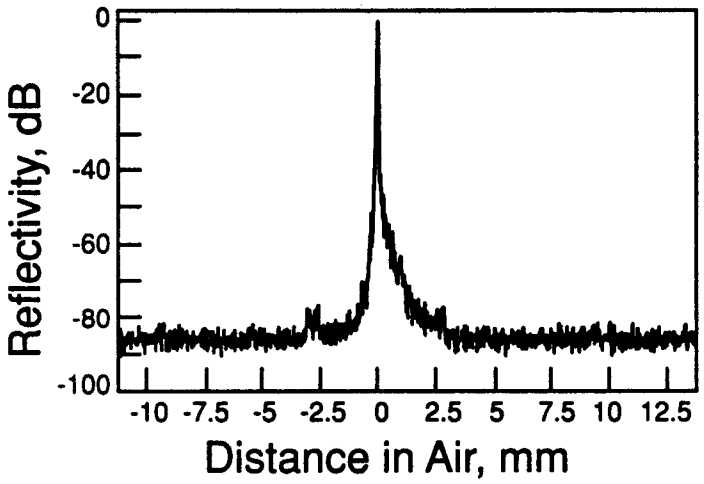

Figure 12

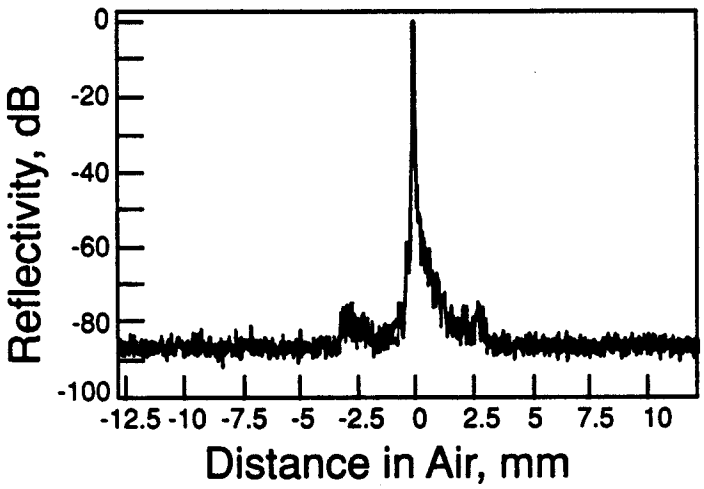

Figure 13a

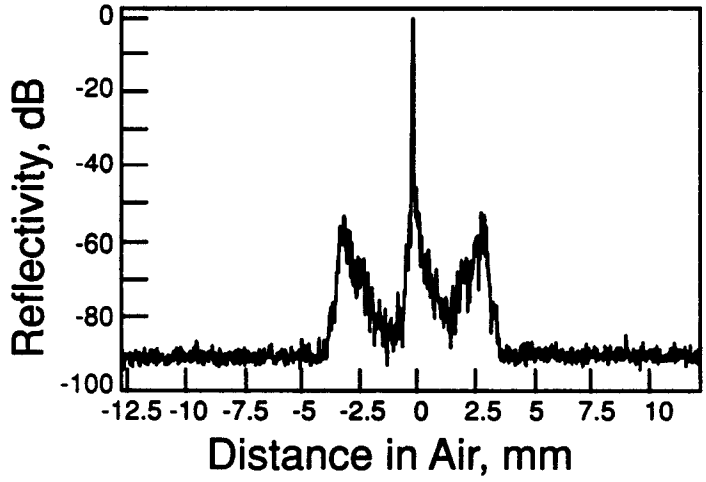

Figure 13b

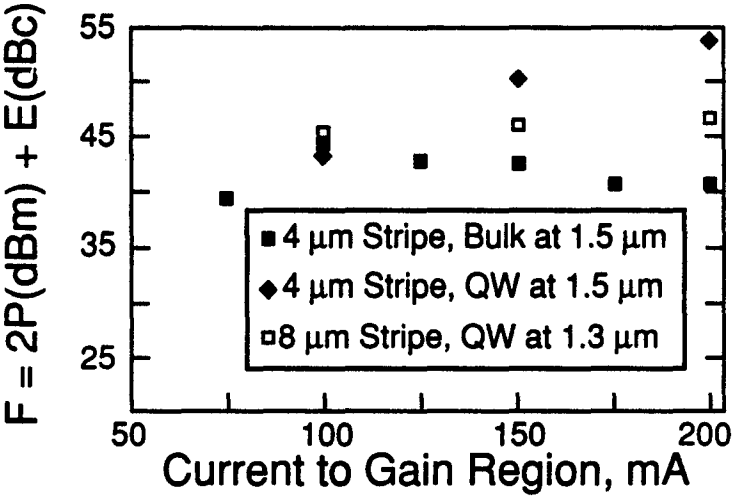
F = 2P(dBm) + E(dBc)
55
45
35
25
50
100
150
200
Current to Gain Region, mA
4 µm Stripe, Bulk at 1.5 µm
4 µm Stripe, QW at 1.5 µm
8 µm Stripe, QW at 1.3 µm

Figure 14

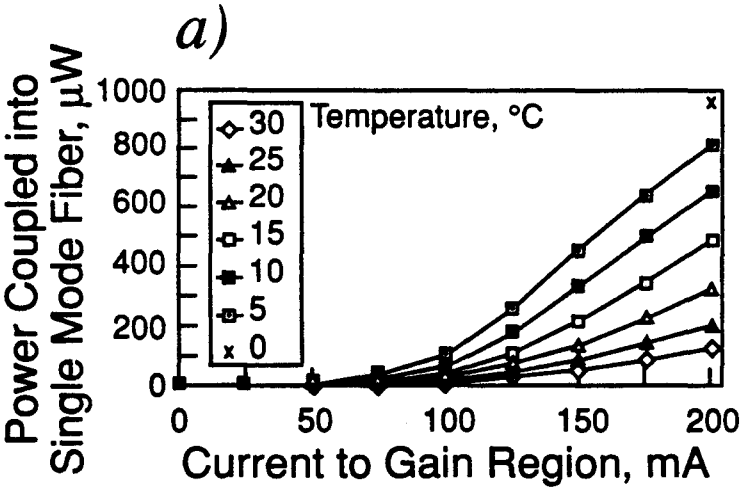

Figure 15a

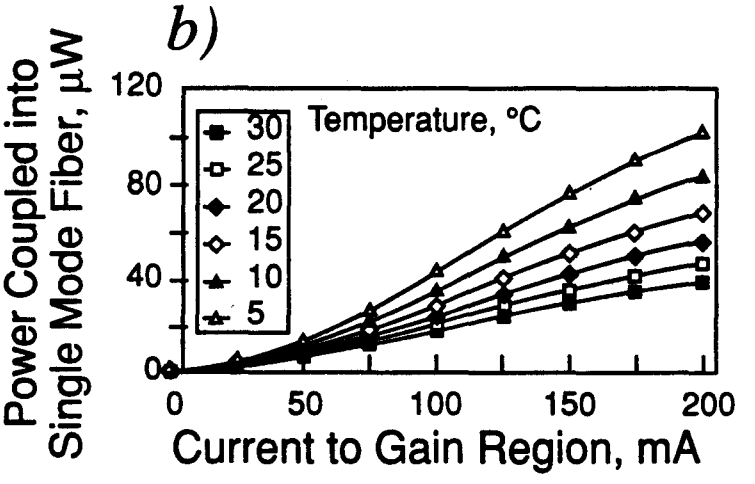

Figure 15b

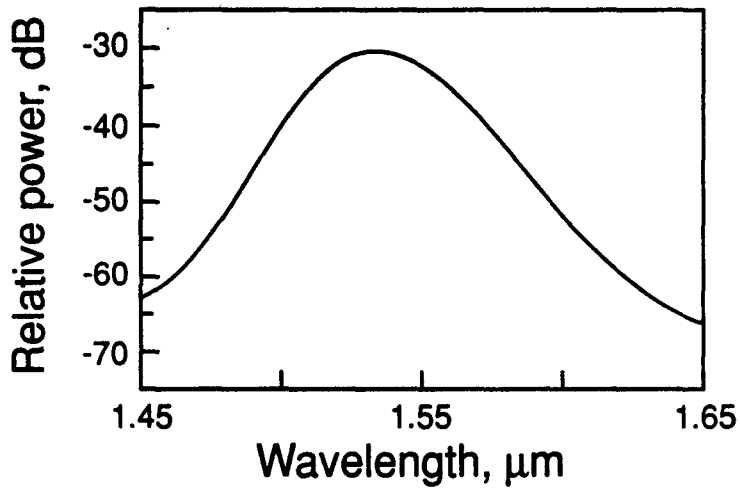

Figure 16